

## Contemporaneous Optical and Near-Infrared Observations of the Interstellar Comet 3I/ATLAS Pre- and Post-Perihelion

KYLE MEDLER <sup>1</sup>, WILLEM B. HOOGENDAM <sup>1,\*</sup>, CHRISTOPHER ASHALL <sup>1</sup>, BIN YANG <sup>2</sup>, JAMES J. WRAY <sup>3,1</sup>,  
BENJAMIN J. SHAPPEE <sup>1</sup>, KAREN J. MEECH <sup>1</sup>, MICHAEL A. TUCKER <sup>4,5</sup>, KATIE AUCHETTL <sup>6,7</sup>, DHVANIL D. DESAI <sup>1</sup>,  
JASON T. HINKLE <sup>8,9,1,†</sup>, ANDREW M. HOFFMAN <sup>1</sup>, MARK E. HUBER <sup>1</sup>, DAVID O. JONES <sup>10</sup> AND RUINING ZHAO <sup>11</sup>

<sup>1</sup>*Institute for Astronomy, University of Hawai'i, 2680 Woodlawn Drive, Honolulu, HI 96822, USA*

<sup>2</sup>*Instituto de Estudios Astrofísicos, Facultad de Ingeniería y Ciencias, Universidad Diego Portales, Santiago, Chile*

<sup>3</sup>*School of Earth and Atmospheric Sciences, Georgia Institute of Technology, 311 Ferst Drive, Atlanta, GA 30332, USA*

<sup>4</sup>*Center for Cosmology and Astroparticle Physics, The Ohio State University, Columbus, OH, USA*

<sup>5</sup>*Department of Astronomy, The Ohio State University, Columbus, OH, USA*

<sup>6</sup>*School of Physics, The University of Melbourne, Parkville, VIC, Australia*

<sup>7</sup>*Department of Astronomy and Astrophysics, University of California, Santa Cruz, CA, USA*

<sup>8</sup>*Department of Astronomy, University of Illinois Urbana-Champaign, 1002 West Green Street, Urbana, IL 61801, USA*

<sup>9</sup>*NSF-Simons AI Institute for the Sky (SkAI), 172 E. Chestnut St., Chicago, IL 60611, USA*

<sup>10</sup>*Institute for Astronomy, University of Hawai'i, 640 N. A'ohoku Pl., Hilo, HI 96720, USA*

<sup>11</sup>*National Astronomical Observatories, Chinese Academy of Sciences, Beijing 100101, China*

### ABSTRACT

Interstellar objects provide a unique view into the formation of other star systems. Here we present spectroscopic observations of the recently discovered interstellar object 3I/ATLAS between a heliocentric distance of 3.7 to 1.8 au on either side of its travels through perihelion. We obtained several observations with the Keck-I/LRIS, Keck-II/NIRES, Gemini/GMOS, and UH88/SNIFS spectrographs, covering a wavelength range of 0.3 – 2.5  $\mu\text{m}$ . We report the continued emission of both Ni and CN, along with post-perihelion detections of Fe and a weak detection of C<sub>3</sub>. We determine the spectral slope across optical and NIR wavelengths and find a positive spectral slope in the optical, with values ranging from  $\sim 21 - 27\%$  in the blue regions (0.4 – 0.55  $\mu\text{m}$ ) to  $\sim 6 - 10\%$  in the red (0.65 – 0.9  $\mu\text{m}$ ) regions. In contrast, the NIR showed a negative spectral slope of  $\sim -0.9\%$  between 0.9 – 1.5  $\mu\text{m}$  and  $\sim -2.3\%$  between 1.9 – 2.5  $\mu\text{m}$ . 3I/ATLAS shows a clear turnover in its spectral shape at  $\sim 1.1 \mu\text{m}$ , corresponding to scattered light from the dusty coma. Finally, in the NIR, we do not find an increase in the depth of the water features identified in an earlier NIR observation of 3I/ATLAS. Our observations of 3I/ATLAS in the NIR show a similar shape to the NIR spectrum of 2I/Borisov as it approached perihelion.

*Keywords:* Asteroids (72) — Comets (280) — Meteors (1041) — Interstellar Objects (52) — Comet Nuclei (2160) — Comet Volatiles (2162)

### 1. INTRODUCTION

Remnant solar system planetesimals (i.e., comets, asteroids, meteors, etc.) serve as probes of the original formation conditions and composition of the Solar System (e.g., E. Bergin et al. 2024). Interstellar objects (ISOs) are extrasolar planetesimals, allowing for the analysis of other solar systems. What makes the study of ISOs so critical is their potential to record the properties of their original solar system,

e.g., providing information on chemical abundances (e.g., D. Jewitt & D. Z. Seligman 2023; A. Fitzsimmons et al. 2024). While it is expected that several ISOs traverse through the solar system at any given time (A. Do et al. 2018), only three have been discovered to date: 1I/'Oumuamua (K. J. Meech et al. 2017), 2I/Borisov (G. Borisov et al. 2019), and, most recently, 3I/ATLAS. 3I/ATLAS was discovered 01 Jul 2025 (L. Denneau et al. 2025) by the Asteroid Terrestrial-impact Last Alert System (ATLAS; J. L. Tonry et al. 2018; J. Tonry et al. 2025). This triggered a global campaign to obtain additional observations (e.g., M. Belyakov et al. 2025; B. Yang et al. 2025; M. A. Cordiner et al. 2025; J. Tonry et al. 2025; D. Hutsemékers et al. 2025; W. B. Hoogendam et al. 2025a).

Corresponding author: Kyle Medler  
kmedler@hawaii.edu

\* NSF Graduate Research Fellow

† NHFP Einstein Fellow

This small sample of observed interstellar objects has shown a diverse range of cometary properties. The first ISO 1I/Oumuamua showed no cometary activity in the form of a dust coma but did exhibit non-gravitational acceleration, similar to the “dark comets” (D. Z. Seligman et al. 2024). In contrast, the second ISO, 2I/Borisov, was significantly more active, with high production rates of gasses including an unusually high CO abundance (relative to H<sub>2</sub>O), > 3 times that of inner solar system comets (e.g., D. Jewitt & D. Z. Seligman 2023; A. Fitzsimmons et al. 2024), as well as a dusty coma (A. Fitzsimmons et al. 2019; P. Guzik et al. 2020; D. Jewitt & J. Luu 2019; C. Opatom et al. 2019).

Compared to the other ISOs, 3I/ATLAS is similar to 2I/Borisov, possessing a large dust coma and high gas production as it approached the sun (D. Z. Seligman et al. 2025; D. Jewitt et al. 2025; M. A. Cordiner et al. 2025; R. de la Fuente Marcos et al. 2025; C. O. Chandler et al. 2025; C. M. Lisse et al. 2025a). Cometary activity has been observed in various wavelength regimes, including water and OH in the UV (Z. Xing et al. 2025), Ni, Fe, C<sub>2</sub>, C<sub>3</sub>, CN, pre-perihelion (R. Rahatgaonkar et al. 2025; D. Hutsemékers et al. 2025; W. B. Hoogendam et al. 2025a; L. E. Salazar Manzano et al. 2025; W. B. Hoogendam et al. 2025b), and post-perihelion CH (W. B. Hoogendam et al. 2026) in the optical, potential water ice in the near-infrared (NIR; B. Yang et al. 2025, see also T. Kareta et al. 2025), CO<sub>2</sub>, CO, H<sub>2</sub>O, and CH<sub>4</sub> in the mid-infrared (M. A. Cordiner et al. 2025; C. M. Lisse et al. 2025a,b; M. Belyakov et al. 2026), and HCN and CH<sub>3</sub>OH (J. T. Hinkle et al. 2025; I. M. Coulson et al. 2025; N. X. Roth et al. 2025) in the sub-mm. Understanding the composition of 3I/ATLAS will provide insights about its formation environment and, therefore, the small bodies and planet-forming environment around another star.

Of particular interest is the water content of 3I/ATLAS. The most abundant solid in proto-planetary discs is water, and it significantly influences planetary formation processes (B. Bitsch & A. Johansen 2016; J. Müller et al. 2021) and likely contributed to giant planet cores (F. J. Ciesla 2014). Furthermore, water is a key ingredient for life in our own Solar System. However, the origin of water on Earth remains debated (for a review, see, e.g., M. Mottl et al. 2007). One model is that comets delivered water to Earth during the heavy bombardment (e.g., C. F. Chyba 1990; K. Meech & S. N. Raymond 2020). This makes understanding the water activity and water content of interstellar objects like 3I/ATLAS important—do other stellar systems contain similar small bodies capable of delivering water to potentially habitable rocky planets?

Both 2I/Borisov and 3I/ATLAS show substantial water production (e.g., B. Yang et al. 2020; Z. Xing et al. 2020; B. Yang et al. 2025; Z. Xing et al. 2025; M. A. Cordiner et al. 2025; M. R. Combi et al. 2025), and dynamical models suggest

3I/ATLAS should be water-rich (M. J. Hopkins et al. 2025). In particular, 3I/ATLAS exhibited a larger inferred water active fraction (i.e., the fraction of the nucleus surface undergoing sublimation) than is typical for many Solar System comets. (Z. Xing et al. 2025; H. Tan et al. 2026). However, both comets showed atypical volatile compositions: 2I/Borisov had a high CO/H<sub>2</sub>O ratio (M. A. Cordiner et al. 2020) and similarly 3I/ATLAS has a high CO<sub>2</sub>/H<sub>2</sub>O ratio (M. A. Cordiner et al. 2025; M. Belyakov et al. 2026). Given the importance of understanding the H<sub>2</sub>O content in interstellar objects, it is natural to turn to the NIR regime that hosts several signatures of water. In particular, the H<sub>2</sub>O 1.5  $\mu$ m absorption and 2.0  $\mu$ m band are readily observed from ground-based facilities and provide direct insights into the water composition of comets. To that end, we present optical to NIR panchromatic observations of 3I/ATLAS obtained by the Hawai‘i Infrared Supernova Study (HISS; K. Medler et al. 2025).

## 2. DATA

We observed 3I/ATLAS using the 10.0 m Keck I and Keck II telescopes, the 8.1 m Frederick C. Gillett Gemini Telescope, and the University of Hawai‘i 88 inch Telescope on Maunakea. The data reduction procedures for each instrument are described below, and an observing log is provided in Table 1. The optical and NIR spectra of 3I/ATLAS are shown in Figure 1.

### 2.1. Optical Observations

Four optical spectra of 3I/ATLAS were obtained over three months, from 26<sup>th</sup> Jul to 30<sup>th</sup> Nov 2025, as it approached and passed perihelion (Oct. 29, 2025 at 1.356 au). The reduction process for each spectrum is detailed below.

#### 2.1.1. LRIS Reductions

Two optical spectra of 3I/ATLAS covering  $\sim 0.3 - 1.0 \mu$ m were obtained on 26.29 Jul 2025 and 27.24 Aug 2025 using the Low-Resolution Imaging Spectrometer (LRIS; J. B. Oke et al. 1995; J. K. McCarthy et al. 1998) mounted on the 10.0-m Keck-I telescope. Observations were taken using the 400/3400 grism and 400/8500 grating. In addition to 3I/ATLAS, observations of two solar analogs were obtained for both epochs, HD 159662 and HD 157378 were obtained for the July observation and HD 146396 and HD 165290 were observed for the August. Finally, a flux calibration star, BD+33 2642, was obtained on the 27<sup>th</sup> of August at a similar airmass to 3I/ATLAS. Due to the limited time available on the 26<sup>th</sup> of July, it was not possible to obtain a flux calibration standard. Instead, the same flux-calibration star from August was used to calibrate both epochs. Comparing the flux of both the comet observations and the observations of the solar analogues from the two epochs, we find agreement between the spectra of the two epochs.

**Table 1.** Log of spectroscopic observations of 3I/ATLAS.  $r_h$  is the heliocentric distance and  $\Delta$  is the geocentric distance.

Instrument	UT Date	$r_h$	$\Delta$	Phase Angle	Solar Analogues	True Anomaly
		[au]	[au]	[Degrees]		[Degrees]
LRIS	2025-07-26	3.68	2.90	11.47	HD 146396/HD 165290	285.4
GMOS	2025-07-27	3.64	2.88	11.91	HD 153631/HD 165290	285.7
GMOS	2025-07-31	3.51	2.82	13.54	HD 153631/HD 165290	286.6
LRIS	2025-08-27	2.66	2.59	22.13	HD 146396/HD 165290	295.5
NIRES	2025-08-28	2.63	2.59	22.31	HD 165290	295.9
SNIFS	2025-11-30	1.79	1.92	30.60	BD +01 2690	44.2
NIRES	2025-11-30	1.79	1.92	30.60	BD +01 2690	44.2

The LRIS observations were reduced using the reduction code `PypeIt` (J. X. Prochaska et al. 2020; J. Prochaska et al. 2020) following the method described in K. Medler et al. (2025). Once the blue and red arms of the LRIS observations were reduced, the arms were stitched together by aligning the high signal-to-noise (S/N) overlapping regions and cutting off the fringe of each arm. Then the combined spectrum was sigma-clipped, while masking regions where emission features from cometary activity lay, to remove low S/N regions at the edges of the grating/grism and to eliminate noise spikes in the data.

#### 2.1.2. GMOS Reduction

Another optical spectrum was obtained by the Gemini-North Multi-Object Spectrograph (GMOS; I. M. Hook et al. 2004) mounted on the 8.1 m Frederick C. Gillette Gemini-North telescope. The observation of 3I/ATLAS was split between two nights, with the first observation obtained on 27.41 Jul using the B480 grating and the second observation occurring on 31.33 Jul with the R150 grating. Alongside observations of 3I/ATLAS, two solar analogues, HD 153631 and HD 165290, were also observed both nights. We flux calibrated the spectrum using a flux-standard star observed at the start of the semester, following standard Gemini operations. Observations of 3I/ATLAS and the two solar analogues were reduced using the automatic reduction pipeline DRAGONS (K. Labrie et al. 2023a,b) version 4.1.0.

#### 2.1.3. SNIFS Reduction

An additional optical spectrum was obtained on 30.61 Nov 2025 by the Supernova Integral Field Spectrograph (SNIFS; B. Lantz et al. 2004) mounted on the University of Hawai'i 88 inch Telescope. The SNIFS instrument is split into two channels, a blue channel which covers 3400–5100 Å range, and a red channel which covers 5100–10000 Å (G. S. Aldering & N. Supernova Factory 2007). The 30.61 Nov 2025 SNIFS

observation was reduced using the standard SCAT pipeline as described in M. A. Tucker et al. (2022).

## 2.2. Infrared Observations

Several NIR spectra were obtained to closely coincide with the optical observations, enabling us to construct, for the first time, a panchromatic time series of spectra of an interstellar object spanning  $\sim 0.33$ – $2.5 \mu\text{m}$  both before and after perihelion.

### 2.2.1. NIRES Reductions

Two NIR spectra, covering  $\sim 0.7$  –  $2.5 \mu\text{m}$ , were obtained by the Hawai'i Infrared Supernova Study (HISS; K. Medler et al. 2025)<sup>1</sup> using the Near-Infrared Echellette Spectrometer (NIRES; J. C. Wilson et al. 2004) on the 10.0-m Keck-II telescope on 28.22 Aug 2025 and 30.66 Nov 2025. The NIRES observations were reduced with the `Spextool` software package (W. D. Vacca et al. 2003; M. C. Cushing et al. 2004) modified for NIRES reductions. Telluric corrections were performed using solar analogue stars in place of the typical A0V star (using the procedures implemented in `xtellcor_general`, see W. D. Vacca et al. 2003, for more information) taken the same night with a similar airmass at the time of observations to that of 3I/ATLAS. The spectral trace in each order was extracted from the NIRES images using an aperture size of  $\sim 1.0''$ . The individual traces were co-added, flux-calibrated, and merged into a single spectrum.

## 3. RESULTS

The panchromatic observations of 3I/ATLAS, presented in Figure 1, show several distinct spectral features. These features range from a strong red optical spectral slope, which is

<sup>1</sup> HISS normally observes supernovae and other astrophysical transients (e.g., W. B. Hoogendam et al. 2025c,d; K. Medler et al. 2025), but the excitement around 3I/ATLAS was contagious!

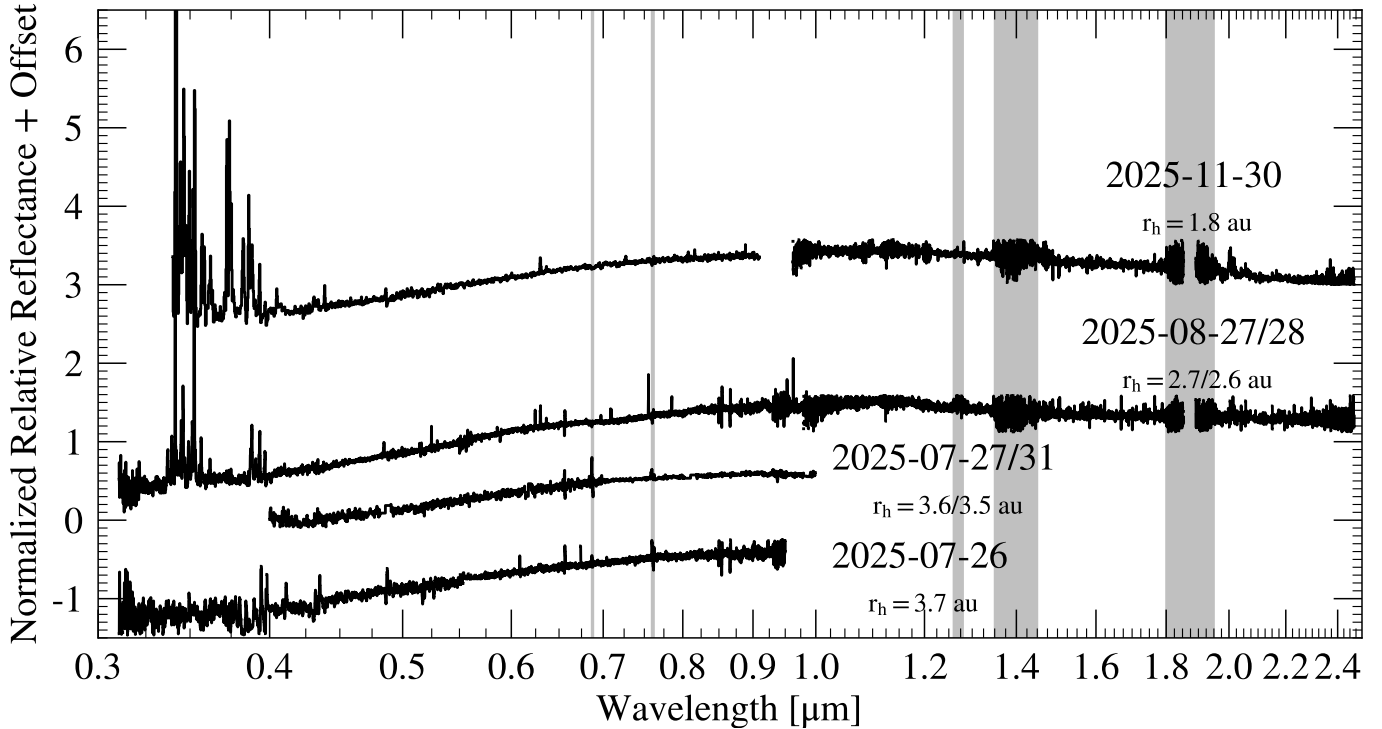


**Figure 1.** Panchromatic reflectance spectra of 3I/ATLAS. All epochs show a clear rising continuum in the optical, peaking around  $1.0 \mu\text{m}$ , indicative of a dusty coma. Between the second and third epochs, strong Ni and CN emission lines appear blueward of  $\sim 0.4 \mu\text{m}$ , with Fe emission lines emerging as 3I/ATLAS made its perihelion passage. All spectra are normalized to reflectance at  $0.5 \mu\text{m}$ , and the telluric regions are denoted by the vertical shaded regions. A zoomed in view on the cometary emission region  $0.33 - 0.5 \mu\text{m}$  is shown in Figure 2.

observed in all spectra, to a transition into a negative spectral slope across the NIR. Additionally, strong emission lines from Ni, Fe,  $\text{C}_3$  and CN are observed on and after Aug 27.24 2025, when 3I/ATLAS was within 2.7 au of the Sun.

To model the production rates of the strong emission features in 3I/ATLAS, we first remove contamination from reflected sunlight. Following R. Rahatgaonkar et al. (2025), W. B. Hoogendam et al. (2025b), and W. B. Hoogendam et al. (2025a), we fit a solar analogue spectrum using the same approach and adopt the following continuum model:

$$F_{\text{cont}}(\lambda) = S \times R(\lambda) \times F_{\odot, \text{ analog}} \left[ \lambda \left( 1 + \frac{v}{c} \right) + \delta\lambda \right], \quad (1)$$

where  $S$  is the normalization factor used to convert the flux of the solar analogue to the same order of magnitude as the 3I/ATLAS spectrum,  $F_{\odot, \text{ analog}}$  is the flux of the solar analogue,  $v$  is the velocity shift between the motion of 3I/ATLAS relative to earth and the solar analogue relative to earth,  $\delta\lambda$  is the wavelength offset between the two spectra, and finally  $R(\lambda)$  is the reflectance function which takes the form of a second order polynomial defined as

$$R(\lambda) = (b_1\lambda^2 + b_2\lambda + 1). \quad (2)$$

This model removes solar absorption features and the dust continuum, enabling us to model the emission features of 3I/ATLAS and determine the production rates of key elements and molecules.

Several emission features emerged in the spectrum of 3I/ATLAS once it had transitioned to a heliocentric distance of  $r_h \leq 2.7$  au. These emission lines are associated with Ni, Fe, CN and CH. The properties of these lines are discussed in the following sections.

### 3.1. Atomic Activity

We examine prominent emission features between 3400 and  $4100 \text{ \AA}$ , which include several atomic and molecular lines associated with outgassing Ni and Fe, as well as  $\text{C}_3$  (W. B. Hoogendam et al. 2025b; R. Rahatgaonkar et al. 2025; D. Hutsemékers et al. 2021). These emission features have been detected in other ISOs (P. Guzik et al. 2020; C. Opitom et al. 2021) and in Solar System objects (J. Manfroid et al. 2021; D. Hutsemékers et al. 2021).

In the July spectra, obtained at  $r_h \approx 3.7-3.5$  au, we do not detect atomic emission lines, indicating that 3I/ATLAS had not yet reached the level of activity required to produce strong metal emission at these distances. By 2025 Aug 27 and 2025 Nov 30, at  $r_h = 2.7$  au and 1.8 au, respectively, we

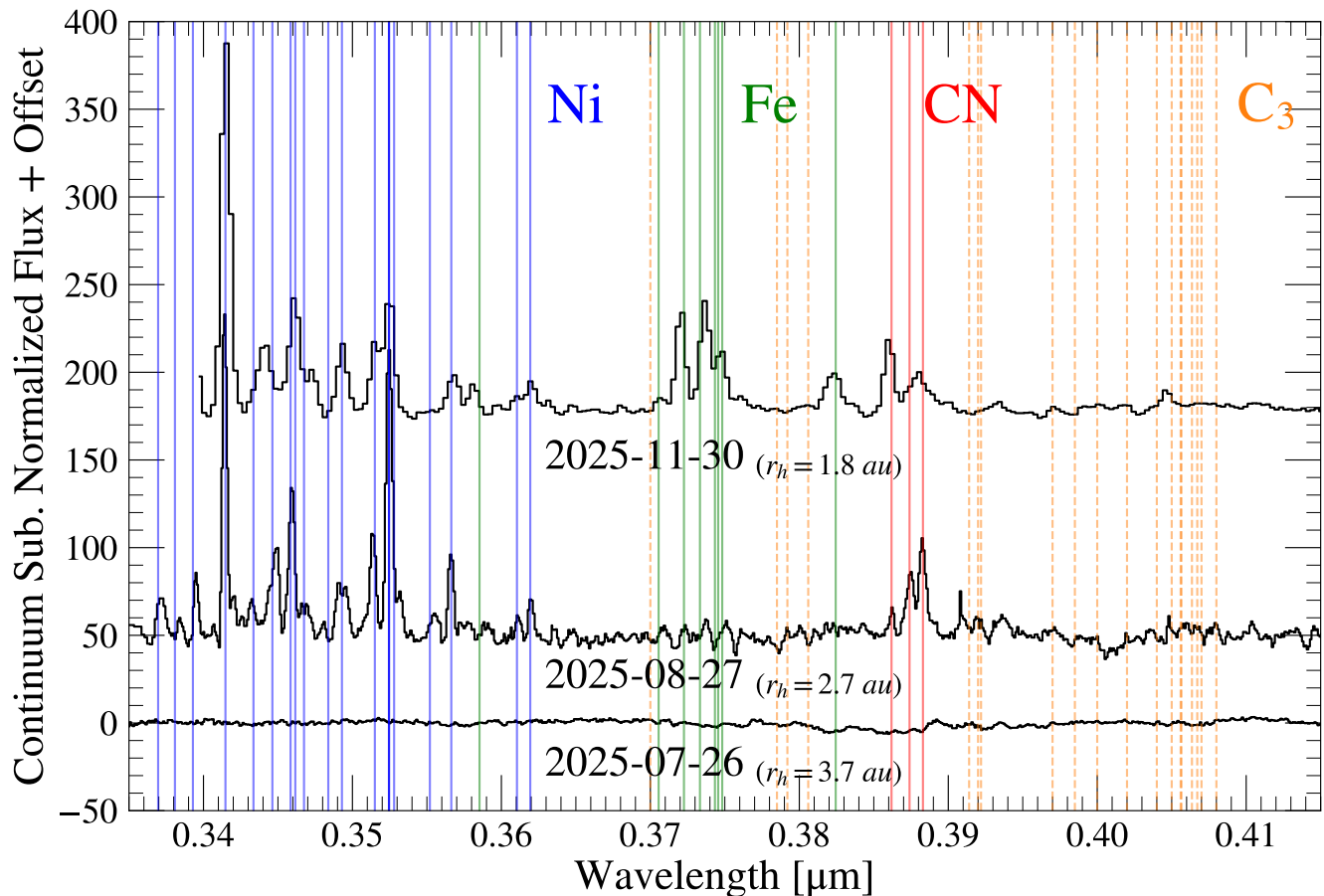


**Figure 2.** Emission lines associated with Ni, Fe, CN, and C<sub>3</sub> that emerge in the LRIS and SNIFS spectra of 3I/ATLAS once it had moved within  $r_h \sim 3$  au. The Fe and C<sub>3</sub> emission lines evolve as 3I/ATLAS approached and past perihelion suggesting a change in the emitting surface. This may have been caused by the Fe-rich material being buried deeper in the surface than the Ni-rich compounds.

detect several strong narrow emission lines from Ni I and Fe I (Figure 2). While Ni I emission lines are clearly detected in the 2025 Aug 27.24 spectrum, the Fe I lines are comparatively weak, although they do seem to be present at this epoch. Such Fe I emission has been observed in Solar System comets at heliocentric distances out to 3.25 au (J. Manfroid et al. 2021).

As noted by R. Rahatgaonkar et al. (2025), the early onset of the Ni I lines, at relatively large heliocentric distances with reduced solar flux, suggests that the Ni does not originate from the sublimation of metallic Ni.

If the Ni I emission does not arise from sublimation of pure metallic Ni, an alternative explanation is the outgassing of Ni from volatile metal carbonyl species from the surface of 3I/ATLAS (S. J. Bromley et al. 2021; J. Manfroid et al. 2021; R. Rahatgaonkar et al. 2025). Additionally, the delay time between the onset of the Ni I lines relative to the Fe I lines can be explained if both the Ni and Fe originate from within carbonyls, such as Ni(CO)<sub>4</sub> and Fe(CO)<sub>5</sub> (J. Manfroid et al. 2021; R. Rahatgaonkar et al. 2025). The delay in Fe I

emission would thus be the result of different sublimation temperatures of Fe carbonyl species compared to the Ni rich carbonyls. This origin for the Ni and Fe in 3I/ATLAS is supported by its evolving Ni I/Fe I ratio, which proved to be highly dependent on the intensity of solar flux and therefore the heliocentric distance of 3I/ATLAS (D. Hutsemékers et al. 2025).

In addition to the Ni and Fe lines that emerge in the spectra of 3I/ATLAS just prior to perihelion, we also observe weak emission features that can be associated with C<sub>3</sub> in the Nov 30<sup>th</sup> 2025 spectrum at  $r_h \approx 1.8$  au, as shown in Figure 2. While we find weak features of C<sub>3</sub>, we do not identify any spectral features associated with either C<sub>2</sub> or CH, which were identified in a spectrum of 3I/ATLAS measured by the Keck Cosmic Web Imager (KCWI) on Nov 16 2025 ( $r_h = 1.5$  au) (W. B. Hoogendam et al. 2026). This is likely due to the weakness of those emission lines and the lower S/N ratio of the SNIFS spectrum relative to the higher resolution KCWI spectrum.

### 3.2. CN production

We identify several emission lines of CN in both the August and November spectra (see Figure 2). These features are noticeably absent from the earlier July spectra. We fit the CN band using a simple Haser model and adopted the parent/daughter scalelengths of  $1.3 \times 10^4 / 2.1 \times 10^5$  km, from M. F. A’Hearn et al. (1995). We adopted the fluorescence efficiency (g-factor; photons per molecule per second) from D. G. Schleicher (2010). The slit width and aperture size for the August CN fit was  $1.0''$  and  $2.21''$  while the November slit width and aperture sizes were  $0.43''$  and  $0.84''$ . From these fits, we find a production rate of CN on Aug 27.24, 2025, to be  $Q(\text{CN}) = 5.7 \pm 1.5 \times 10^{24}$  molecules  $\text{s}^{-1}$ . The CN production rate determined from the Aug 27.24 spectrum is similar to the rates reported in other work, which also observed an increase in activity as 3I/ATLAS approached the sun (R. Rathgaonkar et al. 2025; D. Schleicher 2025; L. E. Salazar Manzano et al. 2025; W. B. Hoogendam et al. 2025b,a). Comparing the CN production rates of the other active ISO shows that 3I/ATLAS ( $5.7 \pm 1.5 \times 10^{24}$  molecules  $\text{s}^{-1}$ ) exhibited a CN production rate roughly twice that of 2I/Borisov ( $3.7 \pm 0.4 \times 10^{24}$  molecules  $\text{s}^{-1}$ ) at a similar heliocentric distance.

In the post-perihelion observation obtained on Nov 30, 2025, the CN production rate increased to  $Q(\text{CN}) = (3.2 \pm 1.2) \times 10^{25}$  molecules  $\text{s}^{-1}$ . This rate is comparable to that measured with TRAPPIST-North around the same epoch (E. Jehin et al. 2025), but is nearly an order of magnitude lower than the value inferred from Keck II/KCWI observations obtained  $\sim 14$  days earlier, when 3I/ATLAS was at  $r_h = 1.5$  au (W. B. Hoogendam et al. 2026). Thus the CN production rate appears to decrease after perihelion passage. A similar trend in the evolution of CN production was also reported from post-perihelion observations of 2I/Borisov (M. A. Cordiner et al. 2020; G. P. Prodan et al. 2024). As 3I/ATLAS moves away from the perihelion, the production rate of CN should continue to decrease as it receives less solar flux. While the post-perihelion trend in CN production rate in both active ISOs is expected, 3I/ATLAS exhibits substantially higher CN abundance than 2I/Borisov (M. A. Cordiner et al. 2020; G. P. Prodan et al. 2024), with  $Q(\text{CN})$  differing by a factor of  $\sim 33$  at comparable heliocentric distances ( $r_h \sim 2.0$  au).

### 3.3. Dust and Coma

At longer wavelengths, the spectrum of 3I/ATLAS is shaped by sunlight scattered by dust in the coma and by molecular emission from rovibrational bands of  $\text{H}_2\text{O}$ , CO, and  $\text{CO}_2$  (M. A. Cordiner et al. 2025). The dust scattering component is prominent in the NIR spectrum presented in this work (Figure 1), where a broad feature peaks near  $\sim 1.15 \mu\text{m}$ . This feature is not apparent in the IRTF spectrum obtained on 2025 Jul 14 (B. Yang et al. 2025), but it is clearly present in

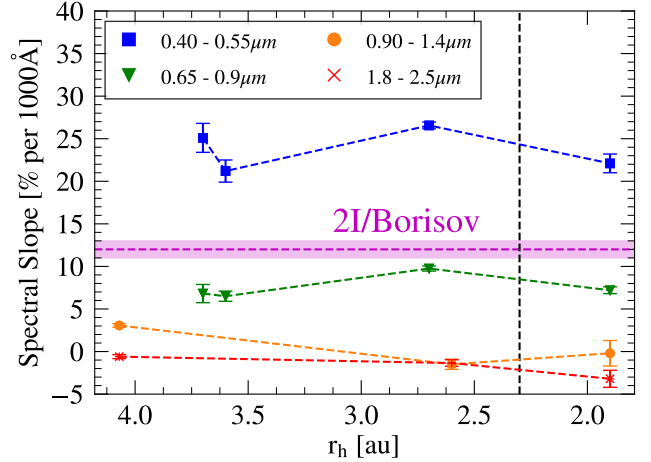


**Figure 3.** Evolution of the optical and NIR spectral slopes of 3I/ATLAS as it approaches perihelion. The dashed vertical line indicates heliocentric distance where 3I/ATLAS crossed perihelion. While the optical slope showed a slight increase in spectral slope between the two Keck-I/LRIS observations, the NIR showed a declining evolution between the initial NIR observation (B. Yang et al. 2025) and the Keck-II/NIRES data. The average optical spectral slope of 2I/Borisov is also included (D. Jewitt & D. Z. Seligman 2023). The spectral slope of 3I/ATLAS is similar to 2I/Borisov between  $0.65 - 0.9 \mu\text{m}$ .

the *JWST* observation acquired  $\sim 23$  days later on 2025 Aug 6 (M. A. Cordiner et al. 2025).

Additionally, in both of the Keck-II/NIRES spectra taken on Aug 28 2025 ( $r_h = 2.6$  au) and Nov 30 2025 ( $r_h = 1.8$  au) we do not detect any strong absorption features associated with  $\text{H}_2\text{O}$ -ice. This is in agreement with the weak features observed in the Jul 14 2025 IRTF spectrum (B. Yang et al. 2025). The lack of any deep  $\text{H}_2\text{O}$  absorption features as 3I/ATLAS moved through perihelion is consistent with sublimation of the previously present surface water ice, or small (micron-sized) ice grains, in agreement with other observations (M. A. Cordiner et al. 2025; B. Yang et al. 2025).

### 3.4. Spectral slope

The shape of the reflectance spectrum of 3I/ATLAS is linked to the object’s physical properties, including its surface composition and volatile driven surface activity. The shape of cometary spectra are commonly quantified using the spectral slope (J. Licandro et al. 2018). To determine the spectral slope of 3I/ATLAS, we correct for the solar continuum by dividing by a solar analogue spectrum and then fit a linear function to the resulting reflectance spectra. The uncertainty on the spectral slope is determined by combining the covariance parameters obtained from the linear fitting and spectral uncertainty in quadrature. The best fit spectral slopes for each wavelength region are listed in Table 2. On 26 Jul 2025, the spectrum had a spectral slope of  $25.1 \pm 1.7\%$  per  $1000 \text{ \AA}$  over  $0.40 - 0.55 \mu\text{m}$  and  $6.8 \pm 1.1\%$  per  $1000 \text{ \AA}$

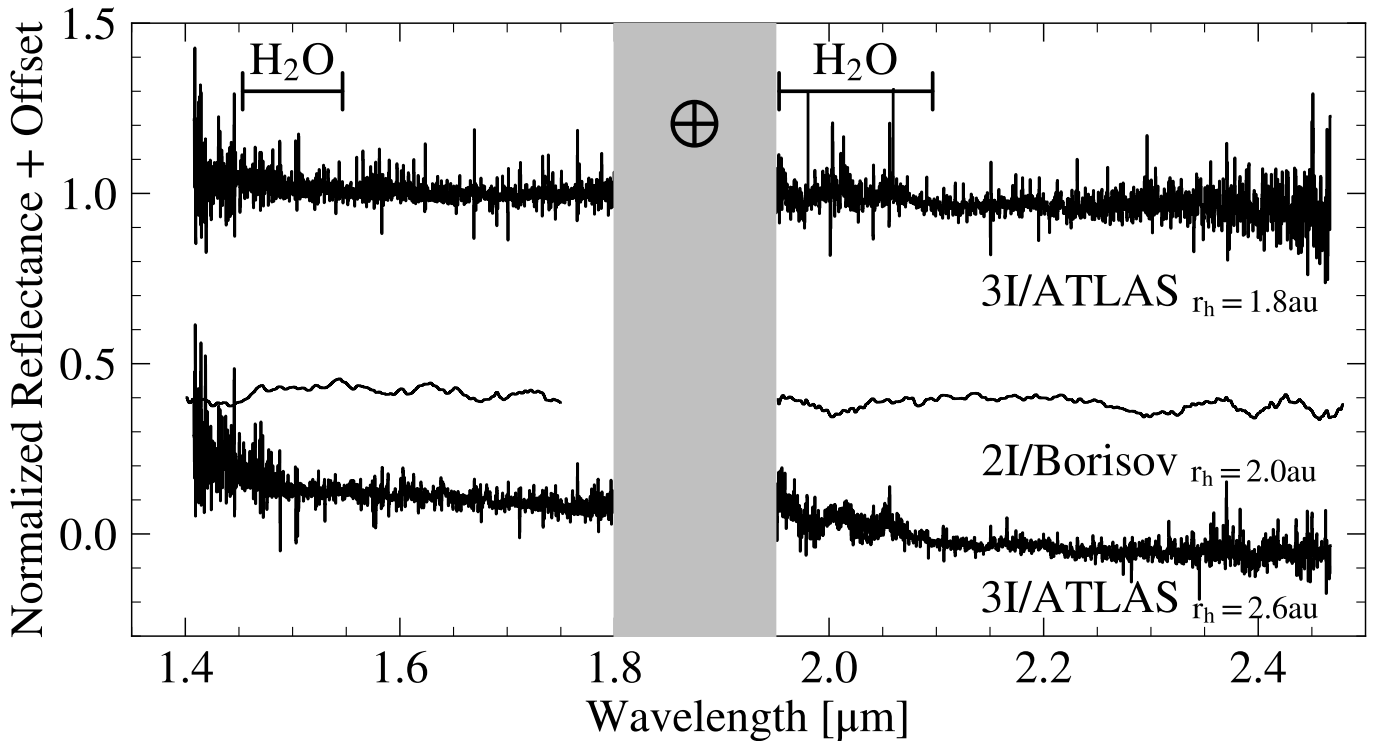


**Figure 4.** Comparison of 3I/ATLAS’s NIR spectrum with the binned NIR spectrum of 2I/Borisov (C.-H. Lee et al. 2020) taken with FLAMINGOS-2 at a heliocentric distance of  $\sim 2.0$  au. Both spectra show a negative spectral slope with no indication of the 1.5 and 2.0  $\mu\text{m}$  H<sub>2</sub>O ice absorption features, which have been highlighted for clarity. The telluric region has been removed from both spectra and marked by the shaded region.

**Table 2.** Spectral slopes determined from fitting a linear function to regions of the optical and NIR spectra

UT Date	Spectral Region [ $\mu\text{m}$ ]	$r_h$ [au]	Spectral Slope [% per 1000 $\text{\AA}$ ]
26 Jul	0.4 – 0.55	3.7	$25.1 \pm 1.7$
	0.65 – 0.9	3.7	$6.8 \pm 1.1$
27 Jul	0.4 – 0.55	3.5	$21.1 \pm 1.3$
31 Jul	0.65 – 0.9	3.5	$6.5 \pm 0.6$
27 Aug	0.4 – 0.55	2.7	$26.6 \pm 0.2$
	0.65 – 0.9	2.6	$9.6 \pm 0.3$
28 Aug	0.9 – 1.5	2.6	$-1.5 \pm 1.1$
	1.4 – 2.0	2.6	$-1.4 \pm 0.4$
30 Nov	0.4 – 0.55	1.8	$22.1 \pm 1.1$
	0.65 – 0.9	1.8	$7.2 \pm 0.4$
	0.9 – 1.4	1.8	$-0.2 \pm 1.5$
	1.9 – 2.5	1.8	$-3.2 \pm 1.0$

over 0.65–0.90  $\mu\text{m}$ . Similar spectral slopes were found in the 27/31 Jul 2025 spectra across the same regions. By 27/28 Aug 2025, at a smaller heliocentric distance, the slopes are  $26.6 \pm 0.2\%$  per 1000  $\text{\AA}$  over 0.40–0.55  $\mu\text{m}$  and  $9.6 \pm 0.3\%$  per

1000  $\text{\AA}$  over 0.65–0.90  $\mu\text{m}$ , indicating no substantial change. The spectral slopes determined from the optical observations are in general agreement with the values determined from other instruments (B. Yang et al. 2025; W. B. Hoogendam et al. 2025b,a), with any discrepancy likely arising from the different wavelength regions used for the fitting. Finally, the spectral slope does not show a significant change between the pre-perihelion observations and the post-perihelion observation taken on 30 Nov 2025. The post-perihelion optical data shows a decreasing spectral slope at redder wavelengths, with the region between 0.4 – 0.55  $\mu\text{m}$  had a slope of  $22.1 \pm 1.1\%$  per 1000  $\text{\AA}$ , which then decreased to  $7.2 \pm 0.4\%$  per 1000  $\text{\AA}$  between 0.65 – 0.9  $\mu\text{m}$ . The post-perihelion NIR observation on 30 Nov 2025 shows a similar trend with a spectral slope of  $-0.2 \pm 1.5$  per 1000  $\text{\AA}$  between 0.9 – 1.4  $\mu\text{m}$  and  $-3.2 \pm 1.0$  per 1000  $\text{\AA}$  across 1.9 – 2.5  $\mu\text{m}$ .

The Keck II/NIRES Aug 28 and Nov 30, 2025 measurements show a significant change from the IRTF and VLT/X-SHOOTER observations obtained at larger heliocentric distances,  $r_h = 4.1$  au and 4.37 au, respectively (B. Yang et al. 2025; A. Alvarez-Candal et al. 2025). The IRTF NIR spectrum shows a spectral slope of  $6.7 \pm 1.4\%$ , whereas the VLT/X-SHOOTER NIR spectrum is too strongly affected by telluric absorption to derive a reliable slope. The difference in NIR slope may reflect increased scattering from dust in

the coma, which likely strengthened between the IRTF and NIRES epochs as 3I/ATLAS approached the Sun. Such an evolution is consistent with rising activity that enhances dust production through volatile-driven outgassing (L. E. Salazar Manzano et al. 2025; M. A. Cordiner et al. 2025). This change in the NIR spectral slope could indicate an increased contribution from pure water ice or hydrated minerals in the coma of 3I/ATLAS (B. Yang et al. 2009). However, we do not detect a corresponding increase in the depths of the H<sub>2</sub>O absorption features near 1.5 and 2.0  $\mu\text{m}$  that were identified in the IRTF spectra, as might be expected if the later spectra were dominated by a more negative slope.

A similar change in the spectral slope was also observed in 2I/Borisov, whose NIR spectral slope evolved from  $\sim 6.0\%$  per 1000  $\text{\AA}$  (B. Yang et al. 2020) to  $\sim -2.2\%$  per 1000  $\text{\AA}$  (C.-H. Lee et al. 2020). The evolution of 2I/Borisov and 3I/ATLAS occurred as they approached perihelion, although the spectral slope of 3I/ATLAS evolved much more rapidly than that of 2I/Borisov. The evolution from a positive to negative spectral slope in 3I/ATLAS occurred between a heliocentric distance of 4.1 au (B. Yang et al. 2025) to 2.6 au, while 2I/Borisov transitioned as the object moved from 2.5 au (B. Yang et al. 2020) to 2.0 au (C.-H. Lee et al. 2020). The turnover in spectral slope observed in 2I/Borisov was suggested to occur as the activity of 2I/Borisov moved from CO-dominant volatiles to H<sub>2</sub>O-dominant volatiles (C.-H. Lee et al. 2020). Both 2I/Borisov and 3I/ATLAS lacked clear H<sub>2</sub>O absorptions at heliocentric distances less than 3 au (Figure 4).

#### 4. CONCLUSIONS

Here, we present panchromatic optical and NIR observations of the interstellar comet 3I/ATLAS. Data were obtained over the course of 6 months as 3I/ATLAS moved from a perihelion distance of 3.7 au to 1.8 au. The optical spectra of 3I/ATLAS show a drastic change between the epochs of observations, with the emergence of a large number of emission features below 0.4  $\mu\text{m}$ . These features are associated with Ni I and Fe I lines and CN emission, along with weak features from C<sub>2</sub> and C<sub>3</sub>. Emission from Fe I lines emerged in the optical spectra of 3I/ATLAS as it approached perihelion and after. From the CN emission feature, we determined a pre-perihelion CN formation rate of  $5.7 \pm 1.5 \times 10^{24}$  molecules s<sup>-1</sup> at a distance of  $\Delta = 2.6$  au /  $r_h = 2.7$  au. The formation rate of CN increased to  $Q(\text{CN}) = 3.2 \pm 1.2 \times 10^{25}$  molecules s<sup>-1</sup> after 3I/ATLAS passed perihelion, at a distance of  $\Delta = 1.9$  au /  $r_h = 1.8$  au. The derived CN formation rate of 3I/ATLAS was an order of magnitude larger than that of the other active interstellar object, 2I/Borisov, suggesting different formation environments, although the nuclear surface area of 3I/ATLAS may also be larger by a similar factor (M.-T. Hui et al. 2026).

We do not identify a clear absorption feature associated with H<sub>2</sub>O-ice at 2.0  $\mu\text{m}$ , although the shape of the NIR spec-

trum around this region is consistent with a weak absorption contaminated by telluric features, making it difficult to measure a H<sub>2</sub>O feature depth. We do not identify the even weaker 1.5  $\mu\text{m}$  absorption feature. We observe a clear evolution in the NIR spectral shape from a positive slope at larger heliocentric distances to a negative slope as 3I/ATLAS moved significantly closer to the Sun. This trend was also observed in 2I/Borisov and in several solar system objects, consistent with an increase in cometary activity as 3I/ATLAS approached the sun. As 3I/ATLAS continues to move past perihelion, H<sub>2</sub>O ice grains could appear in its coma again, so future NIR observations should be obtained to document its continued evolution.

#### ACKNOWLEDGEMENTS

We thank Brian Lemaux and the staff at Gemini North for their assistance in preparing and executing the Gemini Queue observations. We thank Alexa Anderson for helpful discussions of protoplanetary discs.

C.A. and K.M. acknowledge support from NASA grants JWST-GO-02114, JWST-GO-02122, JWST-GO-03726, JWST-GO-04217, JWST-GO-04436, JWST-GO-04522, JWST-GO-05057, JWST-GO-05290, JWST-GO-06023, JWST-GO-06213, JWST-GO-06583, and JWST-GO-06677. Support for these programs was provided by NASA through a grant from the Space Telescope Science Institute, which is operated by the Association of Universities for Research in Astronomy, Inc., under NASA contract NAS5-03127.

W.B.H. acknowledges support from the National Science Foundation Graduate Research Fellowship Program under Grant No. 2236415.

K.J.M., J.J.W., and A.H. acknowledge support from the Simons Foundation through SFI-PD-Pivot Mentor-00009672.

J.T.H. acknowledges support from NASA through the NASA Hubble Fellowship grant HST-HF2-51577.001-A, awarded by STScI. STScI is operated by the Association of Universities for Research in Astronomy, Incorporated, under NASA contract NAS5-26555.

D.O.J. acknowledges support from NSF grants AST-2407632, AST-2429450, and AST-2510993, NASA grant 80NSSC24M0023, and HST/JWST grants HST-GO-17128.028 and JWST-GO-05324.031, awarded by the Space Telescope Science Institute (STScI), which is operated by the Association of Universities for Research in Astronomy, Inc., for NASA, under contract NAS5-26555.

Based on observations obtained at the international Gemini Observatory (program GN-2025B-Q-112), a program of NSF NOIRLab, which is managed by the Association of Universities for Research in Astronomy (AURA) under a cooperative agreement with the U.S. National Science Foundation on behalf of the Gemini Observatory partnership: the U.S.

National Science Foundation (United States), National Research Council (Canada), Agencia Nacional de Investigación y Desarrollo (Chile), Ministerio de Ciencia, Tecnología e Innovación (Argentina), Ministério da Ciência, Tecnologia, Inovações e Comunicações (Brazil), and Korea Astronomy and Space Science Institute (Republic of Korea).

Some of the data presented herein were obtained at Keck Observatory, which is a private 501(c)3 non-profit organization operated as a scientific partnership among the California Institute of Technology, the University of California, and the National Aeronautics and Space Administration. The Obser-

vatory was made possible by the generous financial support of the W. M. Keck Foundation.

This research made use of `PypeIt`<sup>2</sup>, a Python package for semi-automated reduction of astronomical data (J. X. Prochaska et al. 2020; J. X. Prochaska et al. 2020).

*Facilities:* Keck-I(LRIS), Keck-II(NIRES), Gemini(GMOS), UH88(SNIFS)

*Software:* `astropy` (Astropy Collaboration et al. 2013, 2018, 2022), `pypeit` (J. X. Prochaska et al. 2020; J. Prochaska et al. 2020), `spextool` (W. D. Vacca et al. 2003; M. C. Cushing et al. 2004)

## REFERENCES

- A’Hearn, M. F., Millis, R. C., Schleicher, D. O., Osip, D. J., & Birch, P. V. 1995, *Icarus*, 118, 223, doi: [10.1006/icar.1995.1190](https://doi.org/10.1006/icar.1995.1190)
- Aldering, G. S., & Supernova Factory, N. 2007, in *American Astronomical Society Meeting Abstracts*, Vol. 210, American Astronomical Society Meeting Abstracts #210, 82.07
- Alvarez-Candal, A., Rizos, J. L., Lara, L. M., et al. 2025, arXiv e-prints, arXiv:2507.07312, doi: [10.48550/arXiv.2507.07312](https://doi.org/10.48550/arXiv.2507.07312)
- Astropy Collaboration, Robitaille, T. P., Tollerud, E. J., et al. 2013, *A&A*, 558, A33, doi: [10.1051/0004-6361/201322068](https://doi.org/10.1051/0004-6361/201322068)
- Astropy Collaboration, Price-Whelan, A. M., Sipőcz, B. M., et al. 2018, *AJ*, 156, 123, doi: [10.3847/1538-3881/aabc4f](https://doi.org/10.3847/1538-3881/aabc4f)
- Astropy Collaboration, Price-Whelan, A. M., Lim, P. L., et al. 2022, *ApJ*, 935, 167, doi: [10.3847/1538-4357/ac7c74](https://doi.org/10.3847/1538-4357/ac7c74)
- Belyakov, M., Wong, I., Bolin, B. T., et al. 2026, arXiv e-prints, arXiv:2601.22034, doi: [10.48550/arXiv.2601.22034](https://doi.org/10.48550/arXiv.2601.22034)
- Belyakov, M., Fremling, C., Graham, M. J., et al. 2025, arXiv e-prints, arXiv:2507.11720. <https://arxiv.org/abs/2507.11720>
- Bergin, E., Alexander, C., Drozdovskaya, M., Gounelle, M., & Pfalzner, S. 2024, in *Comets III*, ed. K. J. Meech, M. R. Combi, D. Bockelée-Morvan, S. N. Raymond, & M. E. Zolensky, 3–32, doi: [10.2458/azu\\_uapress\\_9780816553631-ch001](https://doi.org/10.2458/azu_uapress_9780816553631-ch001)
- Bitsch, B., & Johansen, A. 2016, *A&A*, 590, A101, doi: [10.1051/0004-6361/201527676](https://doi.org/10.1051/0004-6361/201527676)
- Borisov, G., Durig, D. T., Sato, H., et al. 2019, *Central Bureau Electronic Telegrams*, 4666, 1
- Bromley, S. J., Neff, B., Loch, S. D., et al. 2021, *PSJ*, 2, 228, doi: [10.3847/PSJ/ac2dff](https://doi.org/10.3847/PSJ/ac2dff)
- Chandler, C. O., Bernardinelli, P. H., Jurić, M., et al. 2025, arXiv e-prints, arXiv:2507.13409, doi: [10.48550/arXiv.2507.13409](https://doi.org/10.48550/arXiv.2507.13409)
- Chyba, C. F. 1990, *Nature*, 343, 129, doi: [10.1038/343129a0](https://doi.org/10.1038/343129a0)
- Ciesla, F. J. 2014, *ApJL*, 784, L1, doi: [10.1088/2041-8205/784/1/L1](https://doi.org/10.1088/2041-8205/784/1/L1)
- Combi, M. R., Mäkinen, T., Bertaux, J.-L., et al. 2025, arXiv e-prints, arXiv:2512.22354, doi: [10.48550/arXiv.2512.22354](https://doi.org/10.48550/arXiv.2512.22354)
- Cordiner, M. A., Milam, S. N., Biver, N., et al. 2020, *Nature Astronomy*, 4, 861, doi: [10.1038/s41550-020-1087-2](https://doi.org/10.1038/s41550-020-1087-2)
- Cordiner, M. A., Roth, N. X., Kelley, M. S. P., et al. 2025, arXiv e-prints, arXiv:2508.18209, doi: [10.48550/arXiv.2508.18209](https://doi.org/10.48550/arXiv.2508.18209)
- Coulson, I. M., Kuan, Y.-J., Charnley, S. B., et al. 2025, arXiv e-prints, arXiv:2510.02817, doi: [10.48550/arXiv.2510.02817](https://doi.org/10.48550/arXiv.2510.02817)
- Cushing, M. C., Vacca, W. D., & Rayner, J. T. 2004, *PASP*, 116, 362, doi: [10.1086/382907](https://doi.org/10.1086/382907)
- de la Fuente Marcos, R., Alarcon, M. R., Licandro, J., et al. 2025, *A&A*, 700, L9, doi: [10.1051/0004-6361/202556439](https://doi.org/10.1051/0004-6361/202556439)
- Denneau, L., Siverd, R., Tonry, J., et al. 2025, *MPEC*
- Do, A., Tucker, M. A., & Tonry, J. 2018, *ApJL*, 855, L10, doi: [10.3847/2041-8213/aaae67](https://doi.org/10.3847/2041-8213/aaae67)
- Fitzsimmons, A., Meech, K., Matrà, L., & Pfalzner, S. 2024, in *Comets III*, ed. K. J. Meech, M. R. Combi, D. Bockelée-Morvan, S. N. Raymond, & M. E. Zolensky, 731–766
- Fitzsimmons, A., Hainaut, O., Meech, K. J., et al. 2019, *ApJL*, 885, L9, doi: [10.3847/2041-8213/ab49fc](https://doi.org/10.3847/2041-8213/ab49fc)
- Guzik, P., Drahus, M., Rusek, K., et al. 2020, *Nature Astronomy*, 4, 53, doi: [10.1038/s41550-019-0931-8](https://doi.org/10.1038/s41550-019-0931-8)
- Hinkle, J. T., Yang, B., Meech, K. J., et al. 2025, arXiv e-prints, arXiv:2512.02106, doi: [10.48550/arXiv.2512.02106](https://doi.org/10.48550/arXiv.2512.02106)
- Hoogendam, W. B., Kuesters, D., Shappee, B. J., et al. 2025a, arXiv e-prints, arXiv:2512.09020, doi: [10.48550/arXiv.2512.09020](https://doi.org/10.48550/arXiv.2512.09020)
- Hoogendam, W. B., Shappee, B. J., Wray, J. J., et al. 2025b, arXiv e-prints, arXiv:2510.11779. <https://arxiv.org/abs/2510.11779>
- Hoogendam, W. B., Jones, D. O., Ashall, C., et al. 2025c, *The Open Journal of Astrophysics*, 8, 120, doi: [10.33232/001c.143462](https://doi.org/10.33232/001c.143462)
- Hoogendam, W. B., Ashall, C., Jones, D. O., et al. 2025d, *ApJ*, 988, 209, doi: [10.3847/1538-4357/ade787](https://doi.org/10.3847/1538-4357/ade787)
- Hoogendam, W. B., Jones, D. O., Yang, B., et al. 2026, arXiv e-prints, arXiv:2601.16983. <https://arxiv.org/abs/2601.16983>

<sup>2</sup> <https://pypeit.readthedocs.io/en/latest/>

- Hook, I. M., Jørgensen, I., Allington-Smith, J. R., et al. 2004, *PASP*, 116, 425, doi: [10.1086/383624](https://doi.org/10.1086/383624)
- Hopkins, M. J., Dorsey, R. C., Forbes, J. C., et al. 2025, <https://arxiv.org/abs/2507.05318>
- Hui, M.-T., Jewitt, D., Mutchler, M. J., Agarwal, J., & Kim, Y. 2026, arXiv e-prints, arXiv:2601.21569, doi: [10.48550/arXiv.2601.21569](https://doi.org/10.48550/arXiv.2601.21569)
- Hutsemékers, D., Manfroid, J., Jehin, E., Opitom, C., & Moulane, Y. 2021, *A&A*, 652, L1, doi: [10.1051/0004-6361/202141554](https://doi.org/10.1051/0004-6361/202141554)
- Hutsemékers, D., Manfroid, J., Jehin, E., et al. 2025, arXiv e-prints, arXiv:2509.26053, doi: [10.48550/arXiv.2509.26053](https://doi.org/10.48550/arXiv.2509.26053)
- Jehin, E., Hmiddouch, S., Aravind, K., et al. 2025, *The Astronomer's Telegram*, 17515, 1
- Jewitt, D., Hui, M.-T., Mutchler, M., Kim, Y., & Agarwal, J. 2025, *ApJL*, 990, L2, doi: [10.3847/2041-8213/adf8d8](https://doi.org/10.3847/2041-8213/adf8d8)
- Jewitt, D., & Luu, J. 2019, *ApJL*, 886, L29, doi: [10.3847/2041-8213/ab530b](https://doi.org/10.3847/2041-8213/ab530b)
- Jewitt, D., & Seligman, D. Z. 2023, *ARA&A*, 61, 197, doi: [10.1146/annurev-astro-071221-054221](https://doi.org/10.1146/annurev-astro-071221-054221)
- Kareta, T., Champagne, C., McClure, L., et al. 2025, arXiv e-prints, arXiv:2507.12234. <https://arxiv.org/abs/2507.12234>
- Labrie, K., Simpson, C., Cardenes, R., et al. 2023a, *Research Notes of the American Astronomical Society*, 7, 214, doi: [10.3847/2515-5172/ad0044](https://doi.org/10.3847/2515-5172/ad0044)
- Labrie, K., Simpson, C., Turner, J., et al. 2023b., 3.1.0 Zenodo, doi: [10.5281/zenodo.7776065](https://doi.org/10.5281/zenodo.7776065)
- Lantz, B., Aldering, G., Antilogus, P., et al. 2004, in *Society of Photo-Optical Instrumentation Engineers (SPIE) Conference Series*, Vol. 5249, *Optical Design and Engineering*, ed. L. Mazuray, P. J. Rogers, & R. Wartmann, 146–155, doi: [10.1117/12.512493](https://doi.org/10.1117/12.512493)
- Lee, C.-H., Lin, H.-W., Chen, Y.-T., & Yen, S.-F. 2020, *AJ*, 160, 132, doi: [10.3847/1538-3881/aba8f8](https://doi.org/10.3847/1538-3881/aba8f8)
- Licandro, J., Popescu, M., de León, J., et al. 2018, *A&A*, 618, A170, doi: [10.1051/0004-6361/201832853](https://doi.org/10.1051/0004-6361/201832853)
- Lisse, C. M., Bach, Y. P., Bryan, S. A., et al. 2025a, arXiv e-prints, arXiv:2512.07318. <https://arxiv.org/abs/2512.07318>
- Lisse, C. M., Bach, Y. P., Bryan, S., et al. 2025b, arXiv e-prints, arXiv:2508.15469, doi: [10.48550/arXiv.2508.15469](https://doi.org/10.48550/arXiv.2508.15469)
- Manfroid, J., Hutsemékers, D., & Jehin, E. 2021, *Nature*, 593, 372, doi: [10.1038/s41586-021-03435-0](https://doi.org/10.1038/s41586-021-03435-0)
- McCarthy, J. K., Cohen, J. G., Butcher, B., et al. 1998, in *Society of Photo-Optical Instrumentation Engineers (SPIE) Conference Series*, Vol. 3355, *Optical Astronomical Instrumentation*, ed. S. D'Odorico, 81–92, doi: [10.1117/12.316831](https://doi.org/10.1117/12.316831)
- Medler, K., Ashall, C., Shahbandeh, M., et al. 2025, arXiv e-prints, arXiv:2505.18507, doi: [10.48550/arXiv.2505.18507](https://doi.org/10.48550/arXiv.2505.18507)
- Meech, K., & Raymond, S. N. 2020, in *Planetary Astrobiology*, ed. V. S. Meadows, G. N. Arney, B. E. Schmidt, & D. J. Des Marais, 325, doi: [10.2458/azu\\_uapress\\_9780816540068](https://doi.org/10.2458/azu_uapress_9780816540068)
- Meech, K. J., Weryk, R., Micheli, M., et al. 2017, *Nature*, 552, 378, doi: [10.1038/nature25020](https://doi.org/10.1038/nature25020)
- Mottl, M., Glazer, B., Kaiser, R., & Meech, K. 2007, *Chemie der Erde / Geochemistry*, 67, 253, doi: [10.1016/j.chemer.2007.09.002](https://doi.org/10.1016/j.chemer.2007.09.002)
- Müller, J., Savvidou, S., & Bitsch, B. 2021, *A&A*, 650, A185, doi: [10.1051/0004-6361/202039930](https://doi.org/10.1051/0004-6361/202039930)
- Oke, J. B., Cohen, J. G., Carr, M., et al. 1995, *PASP*, 107, 375, doi: [10.1086/133562](https://doi.org/10.1086/133562)
- Opitom, C., Fitzsimmons, A., Jehin, E., et al. 2019, *A&A*, 631, L8, doi: [10.1051/0004-6361/201936959](https://doi.org/10.1051/0004-6361/201936959)
- Opitom, C., Jehin, E., Hutsemékers, D., et al. 2021, *A&A*, 650, L19, doi: [10.1051/0004-6361/202141245](https://doi.org/10.1051/0004-6361/202141245)
- Prochaska, J., Hennawi, J., Westfall, K., et al. 2020, *The Journal of Open Source Software*, 5, 2308, doi: [10.21105/joss.02308](https://doi.org/10.21105/joss.02308)
- Prochaska, J. X., Hennawi, J., Cooke, R., et al. 2020., v1.0.0 Zenodo, doi: [10.5281/zenodo.3743493](https://doi.org/10.5281/zenodo.3743493)
- Prochaska, J. X., Hennawi, J. F., Westfall, K. B., et al. 2020, *Journal of Open Source Software*, 5, 2308, doi: [10.21105/joss.02308](https://doi.org/10.21105/joss.02308)
- Prochaska, J. X., Hennawi, J., Cooke, R., et al. 2020., v1.0.0 Zenodo, doi: [10.5281/zenodo.3743493](https://doi.org/10.5281/zenodo.3743493)
- Prodan, G. P., Popescu, M., Licandro, J., et al. 2024, *MNRAS*, 529, 3521, doi: [10.1093/mnras/stae539](https://doi.org/10.1093/mnras/stae539)
- Rahatgaonkar, R., Carvajal, J. P., Puzia, T. H., et al. 2025, arXiv e-prints, arXiv:2508.18382, doi: [10.48550/arXiv.2508.18382](https://doi.org/10.48550/arXiv.2508.18382)
- Roth, N. X., Cordiner, M. A., Bockelée-Morvan, D., et al. 2025, arXiv e-prints, arXiv:2511.20845, doi: [10.48550/arXiv.2511.20845](https://doi.org/10.48550/arXiv.2511.20845)
- Salazar Manzano, L. E., Lin, H. W., Taylor, A. G., et al. 2025, arXiv e-prints, arXiv:2509.01647, doi: [10.48550/arXiv.2509.01647](https://doi.org/10.48550/arXiv.2509.01647)
- Schleicher, D. 2025, *The Astronomer's Telegram*, 17352, 1
- Schleicher, D. G. 2010, *AJ*, 140, 973, doi: [10.1088/0004-6256/140/4/973](https://doi.org/10.1088/0004-6256/140/4/973)
- Seligman, D. Z., Farnocchia, D., Micheli, M., et al. 2024, *Proceedings of the National Academy of Science*, 121, e2406424121, doi: [10.1073/pnas.2406424121](https://doi.org/10.1073/pnas.2406424121)
- Seligman, D. Z., Micheli, M., Farnocchia, D., et al. 2025, *ApJL*, 989, L36, doi: [10.3847/2041-8213/adf49a](https://doi.org/10.3847/2041-8213/adf49a)
- Tan, H., Yan, X., & Li, J.-Y. 2026, arXiv e-prints, arXiv:2601.15443, doi: [10.48550/arXiv.2601.15443](https://doi.org/10.48550/arXiv.2601.15443)
- Tonry, J., Denneau, L., Alarcon, M., et al. 2025, arXiv e-prints, arXiv:2509.05562, doi: [10.48550/arXiv.2509.05562](https://doi.org/10.48550/arXiv.2509.05562)
- Tonry, J. L., Denneau, L., Heinze, A. N., et al. 2018, *PASP*, 130, 064505, doi: [10.1088/1538-3873/aabadf](https://doi.org/10.1088/1538-3873/aabadf)
- Tucker, M. A., Shappee, B. J., Huber, M. E., et al. 2022, *PASP*, 134, 124502, doi: [10.1088/1538-3873/aca719](https://doi.org/10.1088/1538-3873/aca719)
- Vacca, W. D., Cushing, M. C., & Rayner, J. T. 2003, *PASP*, 115, 389, doi: [10.1086/346193](https://doi.org/10.1086/346193)

Wilson, J. C., Henderson, C. P., Herter, T. L., et al. 2004, in Society of Photo-Optical Instrumentation Engineers (SPIE) Conference Series, Vol. 5492, Ground-based Instrumentation for Astronomy, ed. A. F. M. Moorwood & M. Iye, 1295–1305, doi: [10.1117/12.550925](https://doi.org/10.1117/12.550925)

Xing, Z., Bodewits, D., Noonan, J., & Bannister, M. T. 2020, ApJL, 893, L48, doi: [10.3847/2041-8213/ab86be](https://doi.org/10.3847/2041-8213/ab86be)

Xing, Z., Oset, S., Noonan, J., & Bodewits, D. 2025, arXiv e-prints, arXiv:2508.04675, doi: [10.48550/arXiv.2508.04675](https://doi.org/10.48550/arXiv.2508.04675)

Yang, B., Jewitt, D., & Bus, S. J. 2009, AJ, 137, 4538, doi: [10.1088/0004-6256/137/5/4538](https://doi.org/10.1088/0004-6256/137/5/4538)

Yang, B., Kelley, M. S. P., Meech, K. J., et al. 2020, A&A, 634, L6, doi: [10.1051/0004-6361/201937129](https://doi.org/10.1051/0004-6361/201937129)

Yang, B., Meech, K. J., Connelley, M., & Keane, J. V. 2025, arXiv e-prints, arXiv:2507.14916. <https://arxiv.org/abs/2507.14916>